Journal of Catalysis 271 (2010) 251–261

Contents lists available at ScienceDirect

Journal of Catalysis

journal homepage: www.elsevier.com/locate/jcat

Catalytic consequences of hydroxyl group location on the rate and mechanism of parallel dehydration reactions of ethanol over acidic zeolites

Hsu Chiang, Aditya Bhan *

Department of Chemical Engineering and Materials Science, University of Minnesota, Twin Cities, 421 Washington Avenue SE, Minneapolis, MN 55455, USA

ARTICLE INFO

Article history:
Received 16 November 2009
Revised 18 January 2010
Accepted 25 January 2010
Available online 6 March 2010

Keywords:
Ethanol dehydration
Zeolite
Mordenite
Ethylene
Diethyl ether
Shape selectivity
Parallel reactions
Size exclusion

ABSTRACT

The effects of zeolite topology on the dehydration of oxygen-containing molecules were probed in steady-state and isotopic chemical reactions of ethanol over proton-form zeolite materials (FER, MFI and MOR) at low temperatures (368–409 K). The measured rate of diethyl ether (DEE) synthesis was largely independent of ethanol partial pressure on all proton-form zeolites (FER, MFI, and MOR), indicating that DEE formation involves the activation of ethanol dimers. The measured rate of DEE synthesis over H-FER increased with increasing ethylene pressure in experiments done with ethanol–ethylene mixtures, reflecting the weaker adsorption of ethanol dimers on the FER framework compared to that on MFI and MOR materials, thereby resulting in the co-adsorption and reaction of ethylene with ethanol on FER materials. Ethylene production was only observed on H-MOR because the small eight-membered ring side pockets protect ethanol monomers from forming bulky ethanol dimers. Secondary kinetic isotopic effects measured for ethylene synthesis rates using C_2D_5OH reactants imply that the kinetically relevant step involves the cleavage of C–O bonds via a carbenium-ion transition state.

1. Introduction

Environmental issues drive the search for alternative sources of fuels and chemicals that are currently derived from petroleum. Plant biomass represents an abundant, carbon-neutral source that can be used to supply energy carriers and chemicals currently produced from crude oil [1]. Since most of plant biomass is comprised of carbohydrates, the intermediates derived from plant biomass typically contain OH groups. The selective removal of these OH groups via dehydration is one of the challenges for production of fuels and chemicals from biomass [2–6].

Proton-form zeolites are solid acid catalysts with channel and pocket dimensions typically less than 1 nm. Zeolite topology can promote reaction rates and selectivity based on spatial constraints [7], attractive or repulsive interactions between adsorbed molecules and pore walls [8,9], and by altering the relative stability of surface-bound intermediates inside mircopores [10]. The microporous host environment in zeolites enables them to be shape-selective catalysts and thus good candidates for selective dehydration of biomass-derived intermediates.

Ethanol dehydration was chosen as a probe reaction to develop a basic understanding of the effects of the size and connectivity of zeolite channels as well as OH group location within zeolite host environments on oxygen removal via dehydration reactions. Ethanol can be dehydrated through a unimolecular route to produce ethylene or through a bimolecular pathway to generate diethyl ether (DEE) [11]. Wang et al. [12] showed that adsorbed ethanol can be dehydrated into a surface-bound ethoxide species on zeolite *H–Y* using solid-state ^{13}C magic-angle spinning (MAS) NMR. In situ infrared spectroscopic studies done by Kondo et al. [13] demonstrated that the desorption of surface-bound ethoxide species on zeolite H-MOR generates ethylene. Kondo et al. [13] introduced ethanol over H-MOR materials at 453 K to decompose ethanol to the surface-bound ethoxide species and water, which was desorbed at 453 K. These authors heated the surface-bound ethoxide species on H-MOR and trapped all the desorbed gas phase species, and subsequently cooled down the temperature to 213 K to re-adsorb the trapped species again. The measured infrared spectrum of the re-adsorbed species at 213 K was nearly identical to the spectrum measured upon exposure to ethylene at 213 K. Zecchina et al. [14] used infrared spectroscopy to study the adsorption of ethanol on H-MOR and H-MFI. Based on the increase in intensity of the background and the Evans window in the infrared spectra, they concluded that two ethanol molecules co-adsorb on the same zeolitic OH group to form an ethanol dimeric species when the ratio of adducts/OH groups was higher than 1:1. The lack of change in the differential heat of adsorption of ethanol (~130 kJ mol^{-1}) at coverages higher than one ethanol molecule per aluminum led Lee et al. [15] to also conclude that dimeric ethanol species are adsorbed on H-ZSM-5. De las Pozas et al. [16] studied ethanol conversion over zeolites H-HEU, H-MFI, H-MOR, H-LTL and H-FAU at

* Corresponding author.
E-mail addresses: chian058@umn.edu (H. Chiang), abhan@umn.edu (A. Bhan).

0021-9517/$ - see front matter © 2010 Elsevier Inc. All rights reserved.
doi:10.1016/j.jcat.2010.01.021

383 K, and their results showed that only H-HEU and H-MOR materials possessing 8-MR channels convert ethanol to ethylene. Ethanol dehydration over zeolites and the effects of zeolite pore topology on ethanol dehydration reactions have already been studied [11,16–22], and the stability and identity of adsorption and reaction intermediates, such as ethanol dimeric species and surface-bound ethoxide species, have been established on the basis of solid-state NMR and infrared spectroscopic studies [12–14] as well as calorimetric measurements [15]. The effects of zeolite topology on the rate and selectivity to ethylene and diethyl ether, however, have not been interpreted in terms of a mechanistic cycle and kinetics for unimolecular and bimolecular ethanol dehydration.

In this work, three zeolite framework materials (H-MFI, H-FER, and H-MOR) were chosen to study the effects of zeolite pore connectivity and channel size on the rate and selectivity of ethanol conversion. The measured kinetic effects of ethanol and ethylene pressure on DEE formation over these three zeolite materials show that ethanol dimers are formed and that these dimeric species are subsequently dehydrated to form DEE. Ethylene formation was only observed on zeolites possessing 8-MR channels because 8-MR channels protect ethanol monomeric species and prevent the formation of ethanol dimeric species due to size restrictions.

2. Materials and methods

2.1. Catalyst preparation

MFI (Si/Al = 42.6, CBV 8014), FER (Si/Al = 11.5, CP 914c), and MOR (Si/Al = 11.1, CBV 21A) zeolite samples from Zeolyst, where the silicon to aluminum ratio was determined by elemental analysis (Galbraith Laboratories), in their NH_4^+ form were sieved to maintain particle sizes between 180 and 425 μm (40–80 mesh) and subsequently treated in dry air (1.67 $cm^3\ s^{-1}$ at NTP conditions, ultrapure, Minneapolis Oxygen) by increasing the temperature from ambient to 773 K at 0.0167 K s^{-1} and holding for 4 h to thermally decompose NH_4^+ to H^+ and $NH_{3(g)}$. The protonated MFI, FER and MOR zeolite samples are abbreviated as H-MFI, H-FER, and H-MOR, respectively.

2.2. Steady-state catalytic reactions of ethanol and ethanol–ethylene mixtures

Steady-state ethanol dehydration reactions were carried out in a tubular packed-bed quartz reactor (10 mm inner diameter) under atmospheric pressure and differential conditions (<1.5% conversion). Catalyst samples (0.005–0.2 g) were supported on a coarse quartz frit inside the reactor, and the temperature was controlled using a furnace (National Electric Furnace FA120 type) connected to a Watlow Temperature Controller (96 series). Catalyst samples weighing less than 0.12 g were diluted with acid-washed quartz particles (0.5–0.8 g, 160–630 μm, European Commission). Catalyst temperatures were measured using a K-type thermocouple touching the bottom of a well on the external surface of the quartz reactor. Catalyst samples were treated in He (1.67 $cm^3\ s^{-1}$, ultrapure, Minneapolis oxygen) at 773 K (0.0167 K s^{-1}) for 3 h prior to cooling in He flow (~1.67 $cm^3\ s^{-1}$) to reaction temperatures (358–409 K). C_2H_5OH (⩾99.5%, Sigma–Aldrich), C_2H_5OD (99.5 at.% D, Sigma–Aldrich) and C_2D_5OD (99.5 at.% D, Sigma–Aldrich) reactants were introduced into flowing gas streams as a liquid using a syringe pump (Cole Parmer 74900 series). Liquid ethanol (2.85×10^{-7}–2.4×10^{-6} mol s^{-1}) was vaporized at 383 K into a gas flow, which contained He (0.55–9.4 $cm^3\ s^{-1}$ at NTP condition) and a mixture of Ar/CH_4 (0.0137–0.0297 $cm^3\ s^{-1}$ at NTP conditions; 75% Ar and 25% CH_4, Minneapolis oxygen) as internal standards; transfer lines were maintained at temperatures greater than 343 K by resistive heating to prevent any condensation. The partial pressure of ethanol was changed by dilution with He (0.55–9.4 $cm^3\ s^{-1}$ at NTP condition, Ultrapure, Minneapolis oxygen). The partial pressures of ethanol and diethyl ether were always kept below their respective vapor pressures at ambient temperature to prevent condensation. Ethylene (0.0053–0.0883 $cm^3\ s^{-1}$ at NTP condition, chemically pure, MATHESON TRI-GAS) was introduced into the reactant stream after ethanol dehydration reactions achieved steady-state. The partial pressure of ethylene (0–1.6 kPa for H-MFI, 0–0.6 kPa for H-MOR and 0–4.5 kPa for H-FER) was changed by adjusting the flow rate of ethylene at a fixed ethanol pressure (1.4 kPa for H-MFI and H-FER; 1.0 kPa for H-MOR). The reactor effluent was sent via heated transfer lines to a mass spectrometer (MKS Cirrus 200 Quadrupole mass spectrometer system) or to a gas chromatograph (Agilent 6890 N GC) equipped with a methyl-siloxane capillary column (HP-1, 50.0 m × 320 μm × 0.52 μm) connected to a flame ionization detector and a packed column (SUPELCO HAYESEP R 80/100 mesh packed column, 12 ft) connected to a thermal conductivity detector. Activation energies and pre-exponential factors were calculated from Arrhenius plots where the reaction rate constants were measured as a function of temperature (358–409 K).

3. Results and discussion

Ethylene and diethyl ether (DEE), products of unimolecular and bimolecular ethanol dehydration reactions, respectively, were observed on H-MOR (Si/Al = 11.1; temperature = 368 K; ethanol pressure = 0.3–6.0 kPa); however, ethanol conversion into ethylene was not observed over H-MFI (Si/Al = 42.6) and H-FER (Si/Al = 11.5) under these reaction conditions as shown in Fig. 1. The concentration of Brønsted acid sites in the three zeolitic materials used for this study was determined by chemical titration using dimethyl ether (DME; see Section S.6. in Supplementary Material). All zeolites used in this study adsorbed 0.5 ± 0.05 DME/Al upon exposure to DME at 438 K, as expected from stoichiometric methylation of hydroxyl groups implying that the concentration of Brønsted acid sites is nearly identical to the concentration of Al in the three zeolites. In the following paragraphs, we present mechanistic cycles for ethanol dehydration over different zeolite materials and interpret these marked effects of zeolite structure on the selectivity of parallel ethanol dehydration reactions in terms of experimentally determined kinetic and thermodynamic parameters.

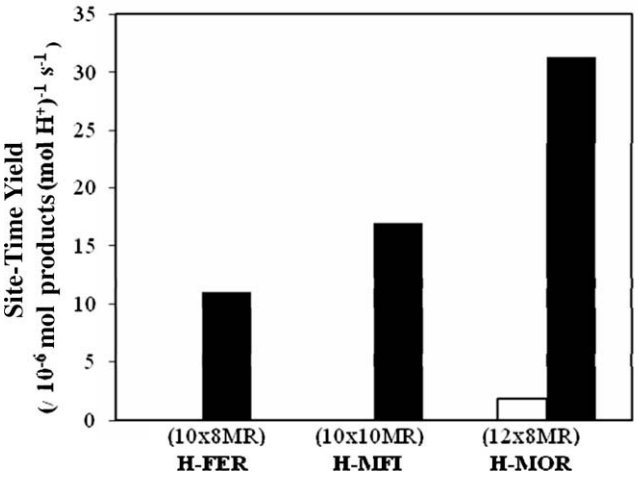

Fig. 1. The rate of DEE (black bars) and ethylene synthesis (white bars) at 368 K and 5 kPa ethanol pressure.

3.1. Kinetics and mechanism for ethanol dimerization into diethyl ether

The measured rates of DEE synthesis over H-FER, H-MFI, and H-MOR as a function of ethanol pressure are shown in Figs. 2–4. The rate of ethanol dimerization over the three zeolite materials increases with increasing ethanol pressure and then gradually approaches an upper limit. Two plausible mechanisms that would account for this observed pressure dependence were proposed for bimolecular ethanol dehydration. The first sequence of elementary steps for ethanol dimerization proposed by Phillips and Datta [11] is dimer-mediated (Scheme 1) and includes ethanol adsorption on a Brønsted acid site to form an ethanol monomer (Step1, Scheme 1) and then co-adsorption of a second ethanol molecule on the same Brønsted acid site to form an ethanol dimer (Step 2, Scheme 1). Subsequent dehydration of the two co-adsorbed molecules forms DEE and water and re-generates the acid site (rate-limiting step, Step 3, Scheme 1). The second sequence of elementary steps for DEE synthesis referred to here as an ethoxide-mediated mechanism includes the adsorption of an ethanol molecule to form an ethanol monomer (Step 1, Scheme 2), and the subsequent decomposition of this ethanol monomer into a surface-bound ethoxide species and water (Step 2, Scheme 2). This ethoxide intermediate subsequently reacts with an ethanol molecule to form DEE (rate-limiting step, Step 3, Scheme 2) and re-generates the Brønsted acid site. The ethanol dimer, which is formed by the co-adsorption of two ethanol monomers (Step 4, Scheme 2), is considered to be an inactive species for the ethoxide-mediated mechanism.

The evidence for the existence of an ethanol dimer and for the surface-bound ethoxide species has already been reported in the literature. Zecchina et al. [14] studied the adsorption of methanol and ethanol over H-ZSM-5 and H-MOR zeolites using infrared spectroscopy. Based on observations in the infrared spectra, when the ratio of adducts/OH groups was higher than 1:1, (i) the intensity of the background and the Evans window increased; (ii) the band centered at 1650–1600 cm^{-1} broadened below 1300 cm^{-1}, and (iii) the intensity of the band at ~2980 cm^{-1} (A component) decreased and the band centered at ~2450 cm^{-1} (B component) broadened, the authors concluded that methanol and ethanol dimers are formed. Furthermore, the lack of change in the differential heat of adsorption of ethanol (~130 kJ mol^{-1}) at coverages higher than one ethanol molecule per aluminum led Lee et al. [15] to conclude that dimeric ethanol species are adsorbed on H-ZSM-5. Adsorbed ethanol can also be decomposed into a surface-bound ethoxide species and water on zeolite *H–Y*. Wang et al. [12] studied the adsorption and activation of ethanol over zeolite *H–Y* using in situ ^{13}C cross-polarization (CP) MAS NMR. Adsorbed ethanol

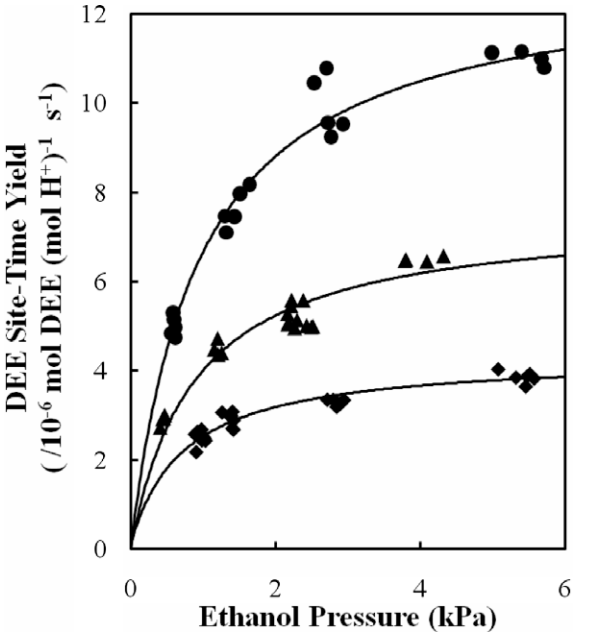

Fig. 2. Measured diethyl ether (DEE) synthesis rate as a function of ethanol pressure over H-FER (Si/Al = 11.5) at 358 K (♦), 363 K (▲) and 368 K (●). The solid lines represent predictions from Eq. (1).

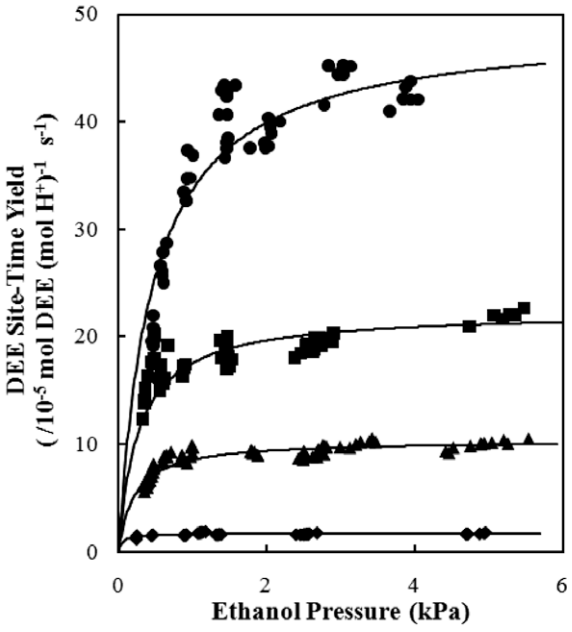

Fig. 3. Measured diethyl ether (DEE) synthesis rate as a function of ethanol pressure over H-MFI (Si/Al = 42.6) at 368 K (♦), 388 K (▲), 398 K (■), and 409 K (●). The solid lines represent predictions from Eq. (1).

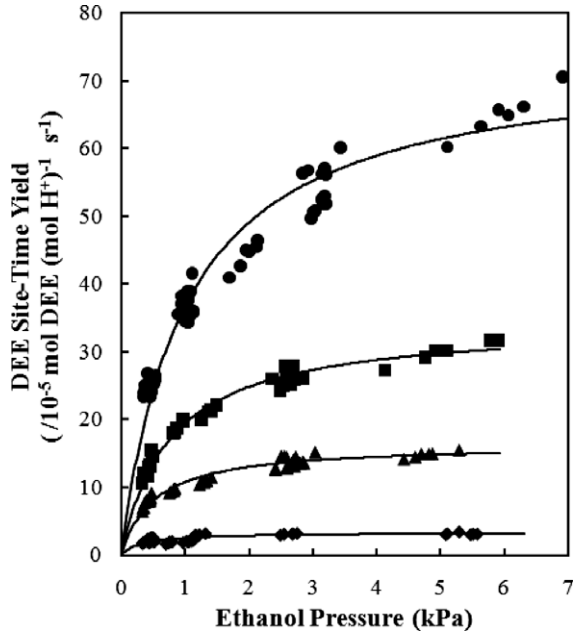

Fig. 4. Measured diethyl ether (DEE) synthesis rate as a function of ethanol pressure for ethanol dehydration over H-MOR (Si/Al = 11.1) at 368 K (♦), 388 K (▲), 398 K (■), and 409 K (●). The solid lines represent predictions from Eq. (1).

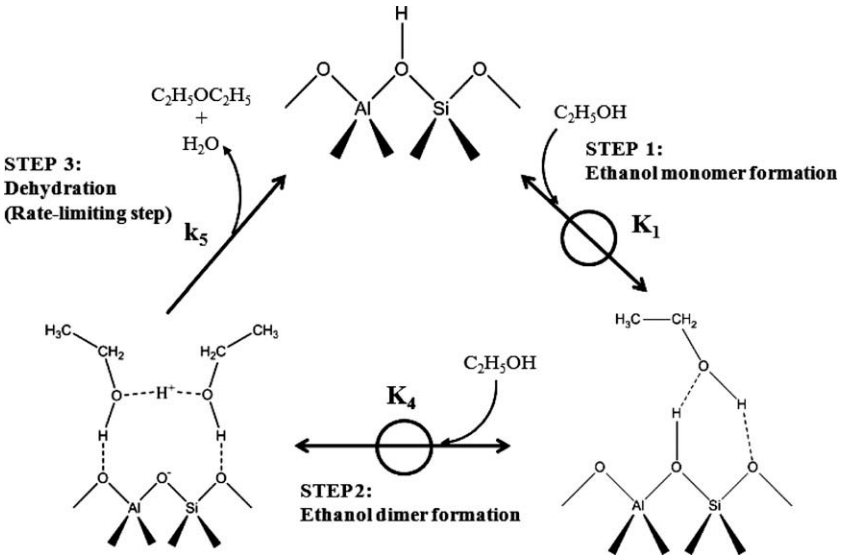

Scheme 1. Proposed elementary steps for ethanol dimerization into diethyl ether via dimer activation over H^+ sites encapsulated in zeolite micropores.

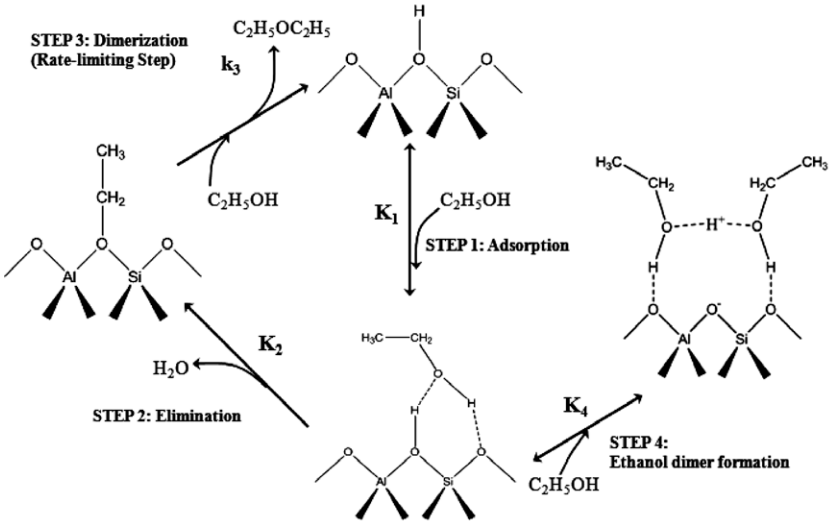

Scheme 2. Proposed mechanism for ethanol conversion into diethyl ether via the formation of surface-bound ethoxide over H^+ sites encapsulated in zeolite micropores.

was heated from 295 K to 453 K. After using dry nitrogen to remove water and physisorbed ethanol at 453 K, a signal was observed at 72.6 ppm due to the formation of a new species. Since this new species could react with water, Wang et al. [12] concluded that this new species is a surface-bound ethoxide species.

Eqs. (1) and (2) are rate laws derived for the dimer-mediated mechanism (Scheme 1) and the ethoxide-mediated mechanism (Scheme 2), respectively, considering dimer activation to form DEE (Step 3, Scheme 1) and the reaction of surface-bound ethoxide species with ethanol to form DEE (Step 3, Scheme 2) to be kinetically relevant (derivations included in the Supplementary Information). Both rate expressions are consistent with the observed zero-order ethanol pressure dependence for ethanol dimerization over the three zeolite materials (shown in Figs. 2–4).

$$\frac{r_{C_2H_5OC_2H_5}}{[H^+]_0} = \frac{k_5K_4[C_2H_5OH]}{1 + K_4[C_2H_5OH]} \quad (1)$$

$$\frac{r_{C_2H_5OC_2H_5}}{[H^+]_0} = \frac{k_3K_2[C_2H_5OH]}{[H_2O] + K_4[H_2O][C_2H_5OH]} \quad (2)$$

The rate parameter k_5 is the intrinsic rate constant for dimer activation (Step 3, Scheme 1); K_4 the adsorption equilibrium constant for ethanol dimer formation (Step 2, Scheme 1 and Step 4, Scheme 2); k_3 the rate constant for the reaction of surface-bound ethoxide species with ethanol (Step 3, Scheme 2) and K_2 is the equilibrium constant for dehydration of the ethanol monomer (Step 2, Scheme 2); $[H^+]_0$ the number of initially accessible Brønsted acid sites and $[C_2H_5OH]$ is the partial pressure of ethanol.

The requirement of ethoxide species for DEE synthesis was probed in ethylene co-feed experiments. If the formation of DEE involves ethoxide species as intermediates (Scheme 2), the rate of DEE synthesis should increase with increasing ethylene pressure because the coverage of ethoxide species increases with increasing pressure of ethylene. The measured rate of DEE synthesis as a function of ethylene pressure over H-MFI (ethanol pressure = 1.4 kPa, ethylene pressure = 0–1.5 kPa, T = 388 K) and H-MOR (ethanol pressure = 1.0 kPa, ethylene pressure = 0–0.57 kPa, T = 409 K) showed that ethylene has no kinetic effect on DEE synthesis rates (Fig. 5a and b) implying that the dimer-mediated mechanism

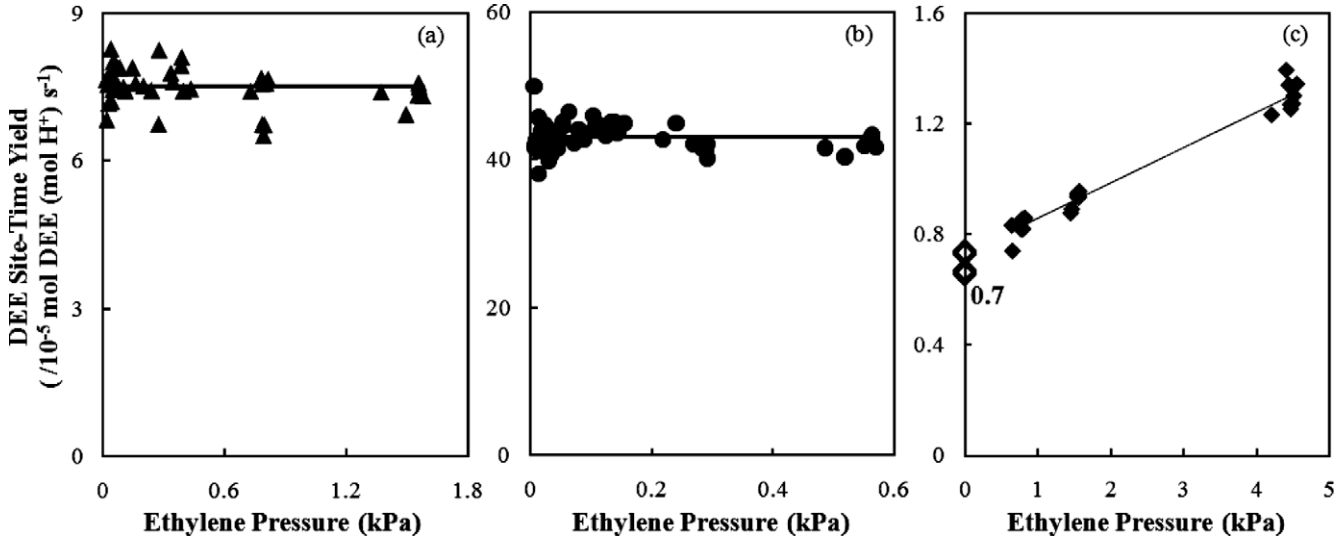

Fig. 5. (a) The rate of DEE synthesis as a function of ethylene pressure over H-MFI (Si/Al = 42.6) at ethanol pressure = 1.4 kPa and T = 388 K (▲), (b) the rate of DEE synthesis as a function of ethylene pressure over H-MOR (Si/Al = 11.1) at ethanol pressure = 1.0 kPa and T = 409 K (●), (c) the rate of DEE synthesis as a function of ethylene pressure over H-FER (Si/Al = 11.5) at ethanol pressure = 1.4 kPa and T = 368 K (♦); the rates of DEE synthesis (average value = 7.0×10^{-6} mol DEE (mol H^+)$^{-1}$ s^{-1}) using only ethanol at ethanol pressure = 1.4 kPa, and T = 368 K (◊).

(Scheme 1) that does not involve ethoxide intermediates is prevalent on H-MFI and H-MOR.

In contrast, the rate of DEE synthesis over H-FER (ethanol pressure = 1.4 kPa, ethylene pressure = 0–4.5 kPa, T = 368 K) increased linearly with increasing ethylene pressure (Fig. 5c). Using the quasi-equilibrium assumption for ethanol monomer and dimer formation and for the formation of ethoxide species formed upon dehydration of the ethanol monomer and upon ethylene adsorption, and the pseudo-steady-state approximation for all reactive intermediates for the ethoxide-mediated mechanism shown in Scheme 2 gave a rate expression for DEE synthesis of the form shown in Eq. (3). The derivation of Eq. (3) is included in the Supplementary Information section.

$$\frac{r_{C_2H_5OC_2H_5}}{[H^+]_0} = \frac{k_3 K_e [C_2H_4]}{K_1 + K_1 K_4 [C_2H_5OH]} \quad (3)$$

where K_e is the equilibrium constant for ethanol adsorption to form the surface-bound ethoxide species; K_1 and K_4 are the equilibrium constants for ethanol monomer and dimer formation, respectively. This equation is inconsistent with the measured effects of ethylene pressure since the regression line has a non-zero intercept (7.5×10^{-6} mol DEE (mol H^+)$^{-1}$ s^{-1}), which is nearly identical to the rate of DEE synthesis (7.0×10^{-6} mol DEE (mol H^+)$^{-1}$ s^{-1}) measured using only ethanol under these reaction conditions (ethanol pressure = 1.4 kPa, T = 368 K) as reported in Fig. 5c. Therefore, the rate equation for ethanol dimerization over H-FER should be comprised of two terms as shown in Eq. (4).

$$\frac{r_{C_2H_5OC_2H_5}}{[H^+]_0} = \frac{k_5 K_4 [C_2H_5OH]}{1 + K_4 [C_2H_5OH]} + \frac{k_{ee} K_{co} [C_2H_4]}{1 + K_4 [C_2H_5OH]} \quad (4)$$

where K_{co} is the equilibrium constant for the formation of co-adsorbed ethylene and ethanol complexes, and k_{ee} is the intrinsic rate constant for activation of the co-adsorbed ethylene and ethanol complex to form diethyl ether. The first term in Eq. (4) represents the contribution from the dimer-mediated mechanism (Scheme 1) and the second term represents the contribution from the activation of a co-adsorbed ethylene and ethanol complex to produce DEE. The co-adsorption of ethanol and ethylene is consistent with the observation that an alkene molecule interacts with an adsorbed methanol molecule to form a co-adsorbed methanol and alkene complex on a zeolitic OH group reported by Svelle et al. [23,24]. These authors used a hybrid MP2:DFT method with a periodically repeated MFI unit cell as a model to investigate the adsorption of ethylene and methanol over zeolite clusters of varying sizes (3–38T) and found that the calculated energy for ethylene co-adsorption (-37 kJ mol^{-1}) on H-ZSM-5 is lower than the heat adsorption of ethylene (-24 kJ mol^{-1} to -31 kJ mol^{-1}).

The activation of co-adsorbed ethylene and ethanol to form DEE may go through two pathways. One is the direct activation of the co-adsorbed ethylene and ethanol complex to form DEE. The second pathway involves the formation of an ethoxide intermediate upon ethylene adsorption and the subsequent reaction of this surface-bound ethoxide with a co-adsorbed ethanol to form DEE (Scheme 3). These two pathways, however, cannot be distinguished kinetically because their corresponding rate expressions have the same form as the second term of Eq. (4).

The kinetic effects of ethylene on the rate of DEE synthesis over MFI, MOR and FER materials leads us to conclude that when only using ethanol as feed, the dimer-mediated mechanism is dominant. This is consistent with the observations made by Blaszkowski and van Santen [25] for conversion of methanol into dimethyl ether on the basis of DFT calculations done on a 3T cluster, which showed that the dimer-mediated mechanism had a lower energy barrier (145 kJ mol^{-1}) compared to the methoxide-mediated mechanism (215 kJ mol^{-1}). The ethanol dimer may alternatively comprise of a protonated ethanol (ethyl oxonium) interacting with a physisorbed ethanol molecule as proposed by Klier et al. for the conversion of alcohols to ethers [26,27]; however, we cannot distinguish between protonated or unprotonated ethanol species on the basis of our reaction studies. In presence of ethylene, the mechanism for DEE formation on FER materials is different than that on MOR and MFI materials, implying that the rate and mechanism for DEE synthesis changes depending on zeolite structure.

Eq. (1) can be written in a linear form as Eq. (5), which accurately describes the kinetic effects of ethanol pressure on DEE formation over the three zeolite materials as shown by the linear dependence of inverse DEE synthesis rates on ethanol pressure (Figs. 6–8). The values of the intrinsic rate constant for dimer activation (k_5, Step 3, Scheme 1) and the equilibrium constant for

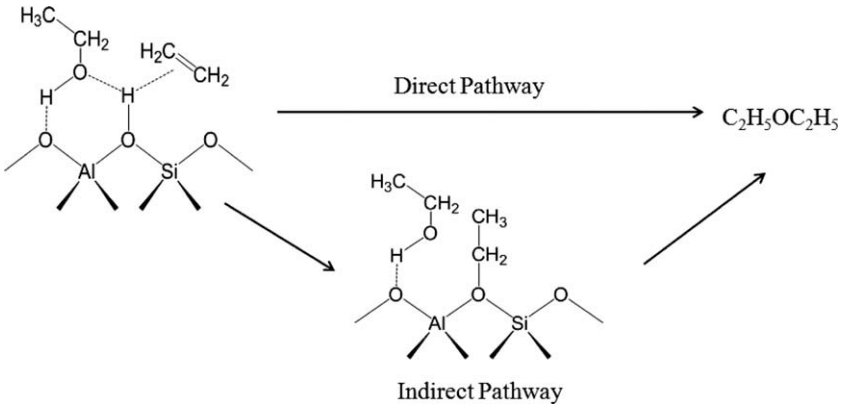

Scheme 3. Direct and indirect routes for activating co-adsorbed ethylene and ethanol to form diethyl ether over FER-type zeolites.

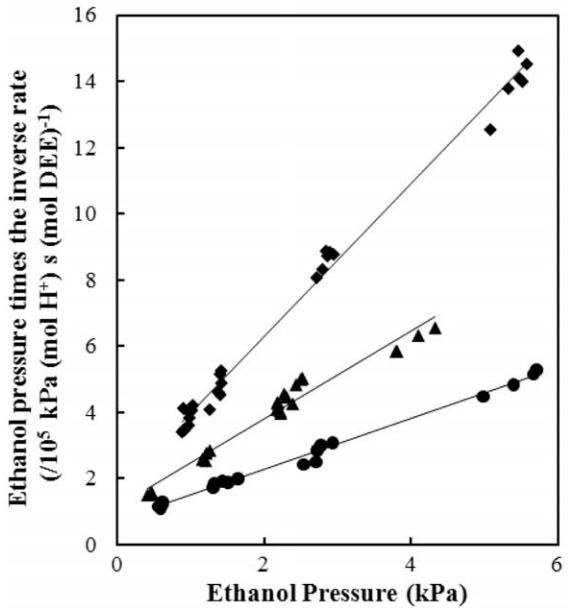

Fig. 6. Ethanol pressure times the inverse rate of diethyl ether (DEE) synthesis as a function of ethanol pressure over H-FER (Si/Al = 11.5) at 358 K (♦), 363 K (▲), and 368 K (●).

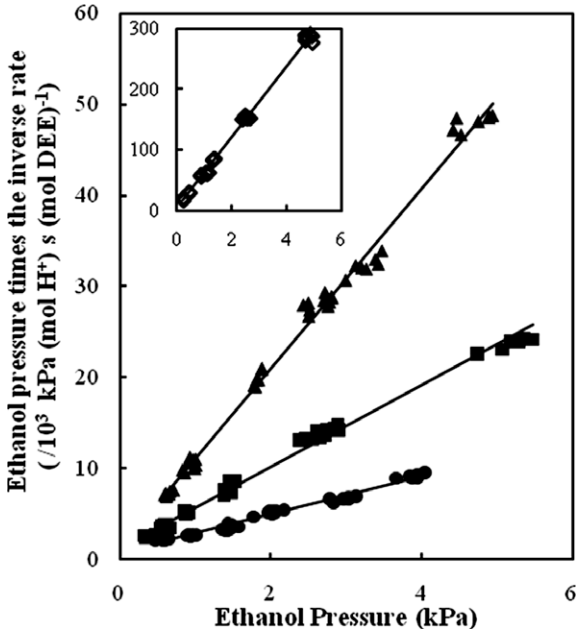

Fig. 7. Ethanol pressure times the inverse rate of diethyl ether (DEE) synthesis as a function of ethanol pressure over H-MFI (Si/Al = 42.6) at 368 K (◇), 388 K (▲), 398 K (■), and 409 K (●).

dimer formation (K_4, Step 2, Scheme 1) can be obtained from the values of the slope and the intercept and are listed in Table 1.

$$\frac{[C_2H_5OH][H^+]_0}{r_{C_2H_5OC_2H_5}} = \frac{1}{k_5K_4} + \frac{[C_2H_5OH]}{k_5} \quad (5)$$

The regressed rate constant for activation of the ethanol dimer (k_5) increases with increasing pore size (H-MOR > H-MFI > H-FER [28]) and the order of regressed equilibrium constants (K_4) is H-MFI > H-MOR > H-FER. The much weaker adsorption of the ethanol dimer in H-FER (K_4 = 107) compared to H-MFI (K_4 = 1859) and H-MOR (K_4 = 313) suggests ethylene can co-adsorb on FER materials and thereby initiate another reaction cycle for DEE synthesis involving the reaction of co-adsorbed ethanol and ethylene in ethylene co-feed experiments described earlier.

3.2. Ethanol dehydration reactions over H-MOR

In this work, ethanol conversion was carried out over H-FER, H-MFI, and H-MOR, however, ethylene production was only observed over H-MOR materials as shown in Fig. 1. The kinetic effects of ethanol pressure on the rate of ethylene synthesis were measured to understand the corresponding mechanism. The data reported in Fig. 9 show that the rate of unimolecular dehydration of ethanol to ethylene decreases with increasing ethanol pressure and that the rate is nearly constant at higher ethanol pressures. This decrease in the rate of unimolecular dehydration of ethanol with increasing ethanol pressure (Fig. 9) is consistent with the observations reported by Macht et al. [29,30] for unimolecular dehydration of 2-butanol over heteropolyacid catalysts (HPA, $H_3PW_{12}O_{40}$). Macht et al. [29,30] attributed the decrease in butanol dehydration rates with increasing 2-butanol pressure to the formation of a 2-butanol dimeric species as inferred from their DFT calculations [31] that showed that the 2-butanol dimer is 84 kJ mol^{-1} more stable than the 2-butanol monomer. Similarly, Lee et al. [32] observed that the rate of unimolecular dehydration of ethanol to ethylene over HPA catalysts ($H_3PW_{12}O_{40}$) also decreased when ethanol pressure increased implying that ethanol dimers formed at high pressures inhibit the rate of ethylene synthesis. The negative kinetic effects of alcohol pressure on unimolecular dehydration rates over HPA catalysts are in agreement with our postulation that the

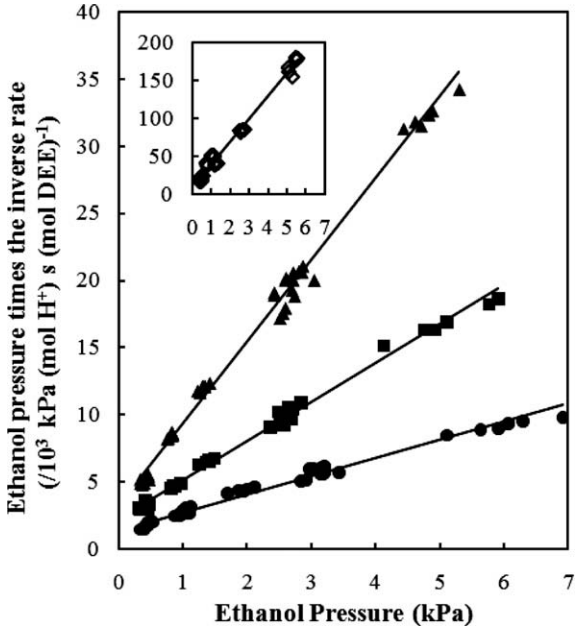

Fig. 8. Ethanol pressure times the inverse rate of diethyl ether (DEE) synthesis as a function of ethanol pressure over H-MOR (Si/Al = 11.1) at 368 K (◇), 388 K (▲), 398 K (■), and 409 K (●).

Table 1
Rate constants (k_5) and adsorption constants (K_4) for DEE synthesis at 368 K over the three types of zeolite frameworks.

Zeolite (Si/Al)	K_4	k_5 ($/10^{-5}$ mol DEE (mol H$^+$)$^{-1}$ s^{-1})
H-FER (11.5)	107	1.3
H-MFI (42.6)	1859	1.7
H-MOR (11.1)	313	3.3

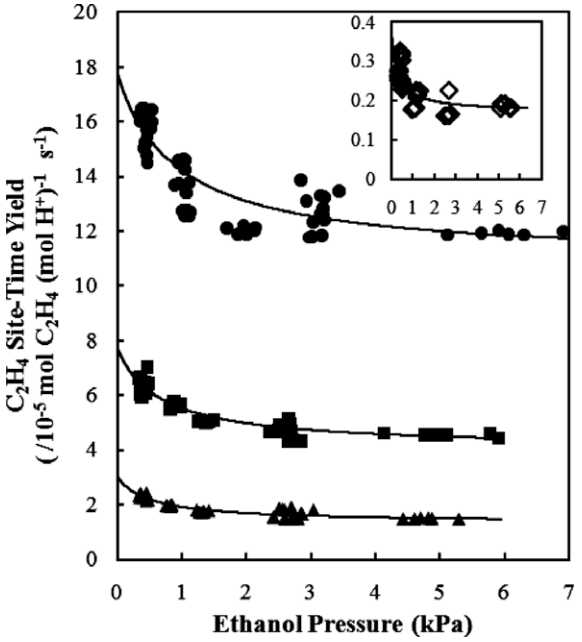

Fig. 9. Ethylene synthesis rate as a function of ethanol pressure over H-MOR (Si/Al = 11.1) at 368 K (◇), 388 K (▲), 398 K (■), and 409 K (●). The solid lines present predictions from Eq. (6).

ethanol dimer inhibits unimolecular dehydration reactions of ethanol over H-MOR.

The rate of ethylene synthesis over H-MOR does not decrease at higher pressures, suggesting that the location of some Brønsted acid sites protects ethanol monomers from forming ethanol dimers. We hypothesize that Brønsted acid sites located in small 8-MR side pockets in H-MOR protect ethanol monomers against the formation of ethanol dimers because of size exclusion; hence, the hydroxyl groups encapsulated in 8-MR pockets can selectively catalyze the unimolecular dehydration of ethanol to ethylene. Indirect evidence that 8-MR channels can prevent the inhibitory effects of ethanol dimeric species on ethylene production can be found in the report by de las Pozas [16]. These authors carried out ethanol conversion over various zeolites (H-HEU, H-FAU, H-LTL, H-MOR and H-MFI) at the vapor pressure of ethanol at 273 K (1.6 kPa) and 383 K, and we note on the basis of selectivity and conversions reported by these authors that only H-HEU and H-MOR, materials that possess 8-MR channels, converted ethanol into ethylene.

Based on the hypothesis that the ethanol dimer is not formed in 8-MR channels, we propose that the mechanism for ethanol dehydration within 8-MR pockets in H-MOR is the same as the mechanism proposed by Kondo et al. [13]. This mechanism includes the adsorption of ethanol on a Brønsted acid site to form an ethanol monomer (Step 1, Scheme 4) and subsequent decomposition of the ethanol monomer to form a surface-bound ethoxide intermediate and water (Step 2, Scheme 4). Desorption of the surface-bound ethoxide intermediate generates ethylene and re-generates the surface Brønsted acid site (Step 3, Scheme 4). The complete catalytic cycle for the conversion of ethanol into ethylene and diethyl ether within 12-MR channels in MOR-type materials is shown in Scheme 5. The mechanism includes the adsorption of ethanol to form an ethanol monomer (Step 1, Scheme 5) and the subsequent decomposition of this ethanol monomer into a surface-bound ethoxide species and water (Step 2, Scheme 5) or the subsequent co-adsorption of another ethanol molecule to form an ethanol dimer (Step 4, Scheme 5). Desorption of the surface-bound ethoxide species generates ethylene (Step 3, Scheme 5) and dimerization of the co-adsorbed ethanol monomers generates diethyl ether and water (Step 5, Scheme 5).

The rate-limiting step for ethanol dehydration mechanisms in 8-MR pockets (Scheme 4) and 12-MR channels (Scheme 5) was probed using isotopic ethanol reactants (C_2H_5OD and C_2D_5OD) at 388 K. The rate of ethylene synthesis using C_2H_5OH is nearly identical to that measured using C_2H_5OD reactants (Table 2; $r_{C_2H_4,H}/r_{C_2H_4,D} = 1.1$; ethanol pressure = 0.46–5.6 kPa; temperature = 388 K); however, the rate of ethylene synthesis decreased when using C_2D_5OD reactants (Table 2, $r_{C_2H_4,H}/r_{C_2H_4,D} = 1.5$) under these reaction conditions. The estimated kinetic isotopic effect (KIE) value at 388 K is ~4.2 for C–H cleavage and ~5.7 for O_{zeo}–H bond cleavage, where O_{zeo} is the oxygen atom in the zeolite lattice; the estimated value of the KIE is ~1.3 for the re-hybridization of the α-carbon from sp^3 to sp^2 hybridization in the transition state for dehydration (Step 2 in Schemes 4 and 5; the estimation of the KIE is discussed in the Supplementary Information). Therefore, the small values of $r_{C_2H_4,H}/r_{C_2H_4,D}$ for both C_2H_5OD and C_2D_5OD reactants show that the rate-limiting step for ethylene production is not the desorption of the ethoxide (Step 3 in Schemes 4 and 5), which involves C–H bond cleavage. The decomposition of adsorbed ethanol into surface-bound ethoxide species and water (Step 2, Schemes 4 and 5) involves O_{zeo}–H bond and C–O bond cleavage. The small values of $r_{C_2H_4,H}/r_{C_2H_4,D}$ for both C_2H_5OD and C_2D_5OD noted earlier imply that this reaction proceeds via a late carbenium-ion-like transition state. The $r_{C_2H_4,H}/r_{C_2H_4,D} = 1.5$ for C_2D_5OD reactants is similar to the estimated value for α-carbon re-hybridization (sp^3–sp^2), indicating that the transition state of the rate-limiting step for ethylene formation involves α-carbon re-hybridization. These observations are consistent with the KIE observed

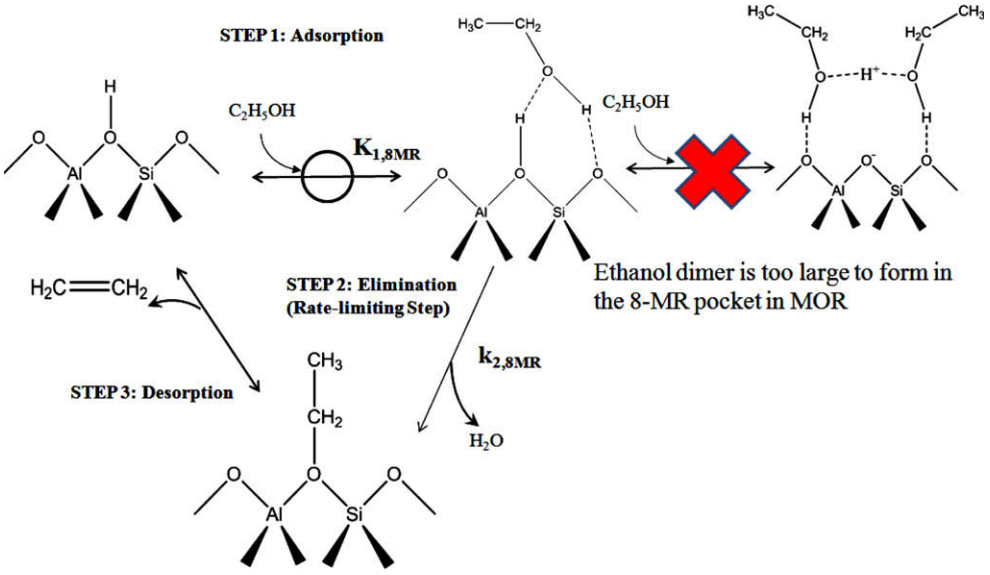

Scheme 4. Proposed elementary steps for ethanol dehydration into ethylene within the 8-MR side pockets in MOR-type zeolites.

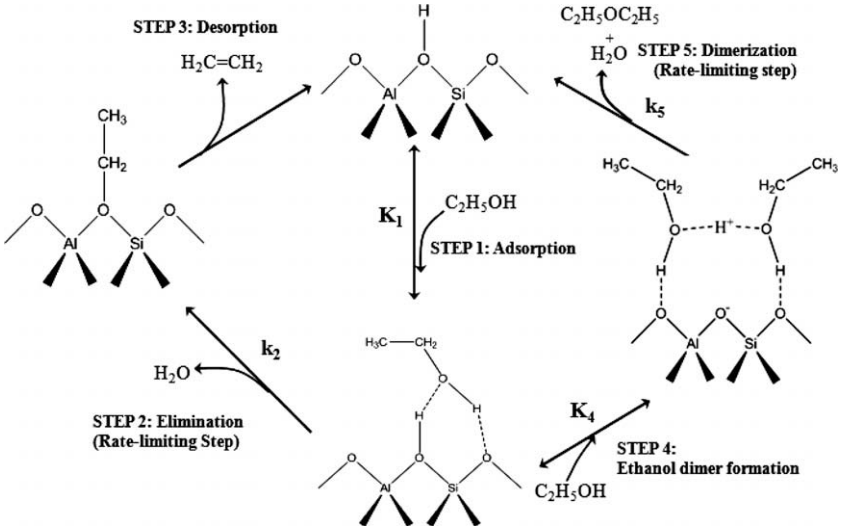

Scheme 5. Proposed mechanism for ethanol conversion into ethylene and diethyl ether in the 12-MR channels in MOR-type zeolites.

Table 2
The measured rates of ethylene synthesis ($r_{C_2H_4}$) using C_2H_5OH (EtOH), C_2H_5OD ($EtOD_1$), and C_2D_5OD ($EtOD_6$) at different pressures at 388 K.

	Pressure (kPa)	$r_{C_2H_4}$ (10^{-5} $(H^+ s)^{-1}$)	$r_{C_2H_4,H}/r_{C_2H_4,D}$[a]
EtOH	2.7	1.8	–
$EtOD_1$	2.8	1.7	1.1
$EtOD_6$	2.8	1.2	1.5
EtOH	4.8	1.5	–
$EtOD_1$	5.6	1.5	1.1
$EtOD_6$	5.2	1.1	1.5
EtOH	0.46	2.3	–
$EtOD_1$	0.53	2.5	0.9
$EtOD_6$	0.51	1.6	1.4

[a] Subscript H means that reactant has no deuterium atoms and subscript D means that the reactant contains deuterium atoms.

for 2-propanol dehydration over HPA catalysts ($H_3PW_{12}O_{40}$) [30]. Macht et al. [30] used CD_3-CHOH-CD_3 and CD_3-CDOD-CD_3 as reactants at 343 K and the measured KIE values reported are 1.6 and 1.4 for CD_3-CHOH-CD_3 and CD_3-CDOD-CD_3, respectively. The secondary KIE values suggest that the transition state for 2-propanol dehydration over HPA catalysts involves the re-hybridization (sp^3–sp^2) of the α-carbon in 2-propanol. These authors also observed that the order of measured rate constants for the dehydration of butanol isomers is 1-butanol (0.09×10^{-3} $(H^+ s)^{-1}$) ≪ 2-butanol (60×10^{-3} $(H^+ s)^{-1}$) ≪ tert-butanol (3300×10^{-3} $(H^+ s)^{-1}$). This order is the same as the order of carbenium-ion stability for the corresponding butanol isomers. In addition, the much larger rate constant of 1-butene isomerization (1.2 $(HPA s)^{-1}$) compared to that of 2-butanol dehydration (0.175 $(HPA s)^{-1}$) in their work suggests that the rate-limiting step is not the desorption of surface-bound butoxide intermediates [29]. Based on the secondary KIE measured for ethanol dehydration over H-MOR as well as the results reported for alkanol dehydration over HPA catalysts in the literature, we conclude that the rate-limiting step for unimolecular dehydration of ethanol in 8-MR pockets and in 12-MR channels in H-MOR is the decomposition of adsorbed ethanol into surface-bound ethoxide species and water (Step 2 in Schemes 4 and 5) via a carbenium-ion transition state.

The rate equation (Eq. (6)) for ethylene synthesis based on the proposed mechanism in 8-MR pockets (Scheme 4) and 12-MR channels (Scheme 5) is consistent with the measured ethanol pressure dependence of ethylene synthesis rates (Fig. 9).

$$\frac{r_{C_2H_4}}{[H^+]_0} = \frac{x_{12MR}k_{2,12MR}}{1 + K_{4,12MR}[C_2H_5OH]} + x_{8MR}k_{2,8MR} \quad (6)$$

where $k_{2,12MR}$ and $k_{2,8MR}$ are the intrinsic rate constants for dehydration of adsorbed ethanol to form surface-bound ethoxide species in 12-MR channels and in 8-MR pockets, respectively; x_{12MR} and x_{8MR} are the fraction of Brønsted acid sites in 12-MR channels and 8-MR pockets, and $K_{4,12MR}$ is the equilibrium constant for ethanol dimer formation inside 12-MR channels.

The values of $K_{4,12MR}$ evaluated from the ethanol pressure dependence of ethylene synthesis rates (Fig. 9) from Eq. (6) are comparable to the values of K_4 evaluated from the ethanol pressure dependence of diethyl ether synthesis rates over H-MOR (Eq. (5); Fig. 8); a tabulated compilation of $K_{4,12MR}$ evaluated from these two independent data sets at different temperatures is reported in Table 3. This consistency in the value of the equilibrium constant for formation of ethanol dimeric species, $K_{4,12MR}$, supports the mechanism proposed in Scheme 5.

No ethylene production is observed on H-MFI because ethanol monomeric species are further converted to energetically favorable ethanol dimers; hence, the dehydration of ethanol results in the formation of diethyl ether instead of ethylene. Ethylene production is only observed on H-MOR among the three zeolites (H-MOR, H-FER, and H-MFI) and the rate of ethylene synthesis does not decrease with increasing ethanol pressure on H-MOR (Fig. 9), suggesting that the 8-MR side pockets are too small to form ethanol dimers. The undetectable ethylene production on H-FER materials is consistent with the observation that most of the Brønsted acid sites are located in the 10-MR channels of H-FER as reported by Eder and Lercher [33] based on the observation that the differential heat of adsorption of n-hexane is constant until the coverage achieved is ~0.9 molecules per acid site.

Zeolites without 8-MR (H-MFI, H-LTL, and H-FAU) channels have also been shown to catalyze the dehydration of ethanol into ethylene at high temperatures (453 K) [16], suggesting that the adsorption of a second ethanol molecule becomes weaker (K_4 becomes small) and the rate constant for ethanol decomposition into surface-bound ethoxide species increases (k_2) at high temperatures. Bun et al. [19] showed that the rate of ethylene synthesis was inversely proportional to ethanol pressure over H-ZSM-5 at high temperatures (543 K) consistent with the rate equation derived from the mechanism shown in Scheme 5 (the first term in Eq. (6)). On the basis of these observations, we suggest that the mechanism for ethanol dehydration within the 12-MR channels of H-MOR (Scheme 5) is also the mechanism for ethanol dehydration over H-MFI. This mechanism is consistent with the zero-order dependence of DEE synthesis rates on ethanol pressure shown in Fig. 3.

The intrinsic rate constant for ethylene synthesis over H-MOR at different temperatures was evaluated by nonlinear regression of Eq. (6) (Fig. 9). The activation energy and pre-exponential for ethylene formation over H-MOR obtained by plotting the natural logarithm of regressed rate constants (k_2) versus the inverse temperature (368–409 K; Fig. 10) are reported in Table 4. The intrinsic activation energy for ethylene synthesis in 8-MR channels is higher than that in 12-MR channels; however, the pre-exponential factor in 8-MR channels is higher than the pre-exponential factor in 12-MR channels. A plausible explanation for this observation is the partial adsorption of the reactant within 8-MR pockets as proposed by Gounder and Iglesia [34] to explain the larger activation energy and entropy of activation for propane dehydrogenation in 8-MR pockets compared to 12-MR channels of H-MOR.

Our results clearly show that bimolecular dehydration of ethanol preferentially occurs in large and medium-pore zeolites; in contrast, spatial constraints imposed by small pores only allow unimolecular dehydration of ethanol. The effects of pore size on unimolecular and bimolecular ethanol dehydration noted in this research resemble the effects of pore size on unimolecular and bimolecular m-xylene disproportionation reported by Clark et al. [35]. These authors used a hybrid quantum mechanical–molecular mechanical (QM/MM) method to determine that over large pore zeolites (H-FAU), the disproportionation reaction of m-xylene can go through either a methoxide-mediated unimolecular pathway or via a diphenylmethane-mediated bimolecular pathway. The formation of diphenylmethane, however, is inhibited in medium-pore

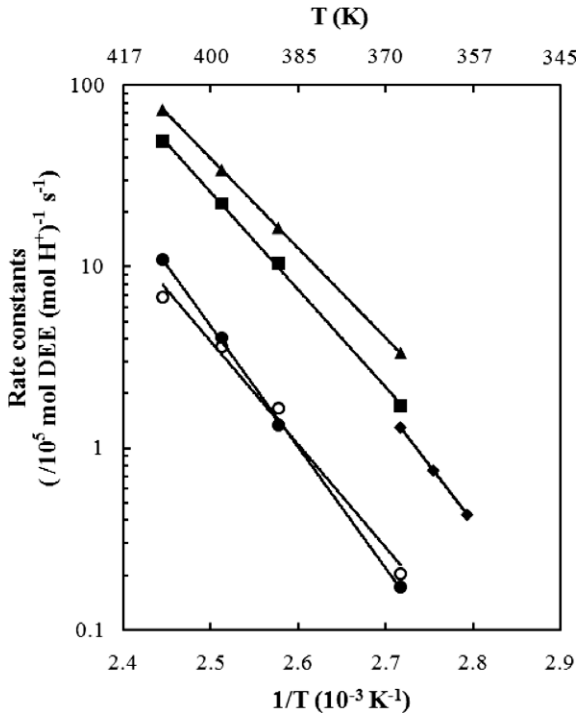

Fig. 10. Measured intrinsic rate constant of DEE synthesis, k_5, over H-FER (♦), H-MFI (■) and H-MOR (▲); measured rate constants of ethylene production by 8-MR pockets (●) and by 12-MR channels (○) in H-MOR.

Table 3
Comparison of the adsorption constant, K_4, from ethylene production data and diethyl ether synthesis data over H-MOR (Si/Al = 11.1).

T (K)	$K_{4,12MR}$ (from C_2H_4)	K_4 (from DEE)
409	108	101
398	150	133
388	191	194
368	332	313

Table 4
Rate constants of ethylene production (k_2) at 388 K, intrinsic activation energy of ethylene synthesis (E_{int}) and pre-exponential factor of ethylene synthesis over the three types of zeolite frameworks. x is the fraction of acid sites in 8-MR pockets or 12-MR channels.

H-MOR	xk_2 (/10^{-5} mol C_2H_4 (mol H^+)$^{-1}$ s^{-1})	E_{int} (kJ mol^{-1})	Pre-exponential factor (mol C_2H_4 (mol H^+)$^{-1}$ s^{-1})
8-MR	1.3	128 ± 10	2.1×10^{12}
12-MR	1.7	109 ± 33	5.8×10^{9}

zeolites (H-MFI and H-MOR) due to steric constraints; hence, the methoxide-mediate pathway is preferred in these materials. These theoretical results reported by Clark et al. [35] are consistent with the intermediates of ethylbenzene disproportionation identified using ^{13}C magic-angle spinning (MAS) NMR by Huang et al. [36]. In large pore H-FAU, the MAS NMR signal of bulky diphenylethane was detected (46 ppm) at 443 K. In medium-pore zeolite materials (H-MOR and H-MFI), surface-bound ethoxide was detected at 483 K (73 ppm), however, no NMR signal corresponding to diphenylethane intermediates was observed.

The effects of the location of zeolitic OH groups on the selectivity of parallel ethanol dehydration reactions, as seen with the 8-MR pockets of H-MOR selectively promoting ethylene synthesis, are in line with recent observations reported by Cheung et al. [37] and Bhan et al. [38,39] for dimethyl ether carbonylation, and by Gounder and Iglesia [34] for parallel reactions of unimolecular alkane activation. Cheung et al. [37,40] noted that the zeolites (H-MOR and H-FER) with eight-membered ring (8-MR) channels had a higher rate of dimethyl ether (DME) carbonylation than zeolites without 8-MR channels (H-BEA, H-FAU and H-MFI). Bhan et al. [38,39] selectively replaced the zeolitic protons in 8-MR side pockets in H-MOR materials with Na^+ cations and noted that the rate of DME carbonylation scaled with the number of Brønsted acid sites within the 8-MR side pockets. Gounder and Iglesia [34] studied the unimolecular cracking and dehydrogenation of propane over H-MOR and Na-MOR at 748 K and showed that rates for both cracking and dehydrogenation of propane within 8-MR pockets are higher than those in 12-MR channels.

The results of ethanol dehydration reactions studied in this research imply that the design and selection of microporous catalysts for performing shape-selective reactions of oxygenates requires us to consider the size and stability of the corresponding surface intermediates as well as the location of Brønsted acid sites.

4. Conclusions

Steady-state ethanol dehydration reactions over H-FER, H-MFI, and H-MOR at 368–409 K showed that H-MOR can catalyze ethanol conversion into both ethylene and diethyl ether, while H-FER and H-MFI can only catalyze bimolecular ethanol dehydration reactions. Ethanol–ethylene co-feed experiments showed that the rate of DEE synthesis over H-MFI and H-MOR is independent of ethylene pressure, suggesting that the mechanism for DEE synthesis involves the dimerization of co-adsorbed ethanol monomers instead of reactions of surface-bound ethoxide species intermediates with ethanol. The measured rates of DEE synthesis over H-FER as a function of ethylene pressure had a regression line where the value of the intercept was nearly identical to the rate of DEE synthesis measured using only ethanol as feed, suggesting that DEE formation on H-FER materials involves both dimerization of co-adsorbed ethanol monomers and the activation of co-adsorbed ethylene and ethanol complexes. No ethylene production is observed on H-MFI and H-FER because ethanol monomeric species are further converted to energetically favorable ethanol dimers.

Ethylene production is only observed on H-MOR among the three zeolites studied (H-MOR, H-FER and H-MFI). The rate of ethylene synthesis does not decrease with increasing ethanol pressure on H-MOR, suggesting that 8-MR side pockets protect ethanol monomers from forming ethanol dimers. Kinetic isotopic effects measured using deuterated ethanol reactants show that the rate-limiting step for ethylene formation is the decomposition of ethanol to form a surface-bound ethoxide species and water via a carbenium-ion transition state. The selectivity to ethylene and diethyl ether in parallel ethanol dehydration reactions is determined by the stability of intermediates, the size of zeolite channels and the location of Brønsted acid sites. In zeolite pores large enough to accommodate ethanol dimers, ethanol preferentially dehydrates via a bimolecular pathway to generate diethyl ether since the formation of ethanol dimeric species is energetically more favorable than the formation of ethanol monomers. In zeolite channels too small to accommodate the ethanol dimer, ethanol is dehydrated via a unimolecular reaction pathway to generate ethylene.

Acknowledgments

The authors acknowledge the financial support from a Discovery Grant from the Institute on the Environment. We also thank Mingwei Tian for assistance with the reaction studies.

Appendix A. Supplementary material

Supplementary data associated with this article can be found, in the online version, at doi:10.1016/j.jcat.2010.01.021.

References

[1] A.T. Bell, B.C. Gates, D. Ray (Eds.), Basic Research Needs: Catalysis for Energy, Reported from US Department of Energy, Basic Energy Sciences Workshop, 2007.
[2] B. Arstad, S. Kolboe, Journal of the American Chemical Society 123 (2001) 8137–8138.
[3] M. Bjorgen, S. Svelle, F. Joensen, J. Nerlov, S. Kolboe, F. Bonino, L. Palumbo, S. Bordiga, U. Olsbye, Journal of Catalysis 249 (2007) 195–207.
[4] R.M. West, D.J. Braden, J.A. Dumesic, Journal of Catalysis 262 (2009) 134–143.
[5] G.W. Huber, A. Corma, Angewandte Chemie – International Edition 46 (2007) 7184–7201.
[6] A. Corma, G.W. Huber, L. Sauvanauda, P. O'Connor, Journal of Catalysis 257 (2008) 163–171.
[7] S.M. Csicsery, Zeolites 4 (1984) 202–213.
[8] F. Eder, M. Stockenhuber, J.A. Lercher, Journal of Physical Chemistry B 101 (1997) 5414–5419.
[9] T.F. Degnan, Journal of Catalysis 216 (2003) 32–46.
[10] M.W. Anderson, J. Klinowski, Journal of the American Chemical Society 112 (1990) 10–16.
[11] C.B. Phillips, R. Datta, Industrial & Engineering Chemistry Research 36 (1997) 4466–4475.
[12] W. Wang, J. Jiao, Y.J. Jiang, S.S. Ray, M. Hunger, Chemphyschem 6 (2005) 1467–1469.
[13] J.N. Kondo, K. Ito, E. Yoda, F. Wakabayashi, K. Domen, Journal of Physical Chemistry B 109 (2005) 10969–10972.
[14] A. Zecchina, S. Bordiga, G. Spoto, D. Scarano, G. Spano, F. Geobaldo, Journal of the Chemical Society – Faraday Transactions 92 (1996) 4863–4875.
[15] C.C. Lee, R.J. Gorte, W.E. Farneth, Journal of Physical Chemistry B 101 (1997) 3811–3817.
[16] C. de las Pozas, R. Lopez-Cordero, J.A. Gonzalez-Morales, N. Travieso, R. Roque-Malherbe, Journal of Molecular Catalysis 83 (1993) 145–156.
[17] J.C. Oudejans, P.F. Vandenoosterkamp, H. Vanbekkum, Applied Catalysis 3 (1982) 109–115.
[18] R. Levanmao, T.M. Nguyen, G.P. McLaughlin, Applied Catalysis 48 (1989) 265–277.
[19] S. Bun, S. Nishiyama, S. Tsuruya, M. Masai, Applied Catalysis 59 (1990) 13–29.
[20] I. Takahara, M. Saito, M. Inaba, K. Murata, Catalysis Letters 105 (2005) 249–252.
[21] D. Varisli, T. Dogu, G. Dogu, Chemical Engineering Science 62 (2007) 5349–5352.
[22] Q.J. Zhu, J.N. Kondo, S. Inagaki, T. Tatsumi, Topics in Catalysis 52 (2009) 1272–1280.
[23] S. Svelle, S. Kolboe, O. Swang, U. Olsbye, Journal of Physical Chemistry B 109 (2005) 12874–12878.
[24] S. Svelle, C. Tuma, X. Rozanska, T. Kerber, J. Sauer, Journal of the American Chemical Society 131 (2009) 816–825.
[25] S.R. Blaszkowski, R.A. van Santen, Journal of the American Chemical Society 118 (1996) 5152–5153.
[26] K. Klier, Topics in Catalysis 18 (2002) 141–156.
[27] K. Klier, Q. Sun, O.C. Feeley, M. Johansson, R.G. Herman, in: J.W. Hightower, W.N. Delgass, E. Iglesia, A.T. Bell, (Eds.), 11th International Congress on Catalysis – 40th Anniversary, Pts a and B., pp. 601–610.
[28] IZA Structure and Commission, <http://www.iza-structure.org/>.
[29] J. Macht, M.J. Janik, M. Neurock, E. Iglesia, Angewandte Chemie – International Edition 46 (2007) 7864–7868.
[30] J. Macht, M.J. Janik, M. Neurock, E. Iglesia, Journal of the American Chemical Society 130 (2008) 10369–10379.
[31] M.J. Janik, J. Macht, E. Iglesia, M. Neurock, Journal of Physical Chemistry C 113 (2009) 1872–1885.

[32] K.Y. Lee, T. Arai, S. Nakata, S. Asaoka, T. Okuhara, M. Misono, Journal of the American Chemical Society 114 (1992) 2836–2842.
[33] F. Eder, J.A. Lercher, Journal of Physical Chemistry B 101 (1997) 1273–1278.
[34] R. Gounder, E. Iglesia, Journal of American Chemical Society 131 (2009) 1958–1971.
[35] L.A. Clark, M. Sierka, J. Sauer, Journal of the American Chemical Society 126 (2004) 936–947.
[36] J. Huang, Y. Jiang, V.R.R. Marthala, M. Hunger, Journal of the American Chemical Society 130 (2008) 12642-+.
[37] P. Cheung, A. Bhan, G.J. Sunley, D.J. Law, E. Iglesia, Journal of Catalysis 245 (2007) 110–123.
[38] A. Bhan, A.D. Allian, G.J. Sunley, D.J. Law, E. Iglesia, Journal of the American Chemical Society 129 (2007) 4919–4924.
[39] A. Bhan, E. Iglesia, Accounts of Chemical Research 41 (2008) 559–567.
[40] P. Cheung, A. Bhan, G.J. Sunley, E. Iglesia, Angewandte Chemie – International Edition 45 (2006) 1617–1620.